

# Analytic approach to dielectric optical bent slab waveguides

K. R. Hiremath, M. Hammer, R. Stoffer

MESA<sup>+</sup> Research Institute, University of Twente, Enschede, The Netherlands

L. Prkna, J. Čtyroký

Institute of Radio Engineering and Electronics AS CR, Prague, Czech Republic

July 19, 2005

## Abstract

A rigorous classical analytic model of confined optical wave propagation along 2-D bent slab waveguides and curved dielectric interfaces is investigated, based on a piecewise frequency domain ansatz for bend mode profiles in terms of Bessel and Hankel functions. This approach provides a clear picture of the behaviour of bend modes, concerning their decay for large radial arguments or effects of varying bend radius. Fast and accurate routines are required to evaluate Bessel functions with large complex orders and large arguments. Our implementation enabled detailed studies of bent waveguide properties, including higher order bend modes and whispering gallery modes, their interference patterns, and issues related to bend mode normalization and orthogonality properties.

## 1 Introduction

Bent dielectric waveguides play an important role in photonic integrated circuits. Accurate evaluation of mode profiles, phase propagation constants, and of optical losses associated with the leaky wave propagation is the central task for theoretical modeling of the curved structures. The present work on this — rather old — topic is motivated by the recent interest in circular optical microresonator devices as building blocks for large-scale integrated optics [1, 2]. During our participation in a related European project [3], we experienced that certain notions about the properties of bend modes deserved clarification. This concerns e.g. the behaviour of the mode profiles for large radial coordinates, profile integrability, mode orthogonality, or a clear picture of propagation and interference of the bend modes.<sup>1</sup>

A sound modal analysis of bent slabs becomes particularly relevant if the mode profiles are to be employed as basis fields for a description of integrated optical microresonators with circular, ring- or disk-shaped cavities. In a framework of coupled mode theory [4, 5, 6], an as far as possible analytic representation of the basic field profiles on a radially unbounded domain must be regarded as highly advantageous. This is provided by the approach followed in this paper. Preliminary promising studies are contained in [7, 8, 9]; further details will be published elsewhere (see e.g. [10] for steps towards a 3D generalization).

Initial models of optical bent waveguides can be found in [11, 12]. Since then, various different techniques were applied to the task. By conformal mapping [13, 14], the bent waveguide problem can be transformed into equations for a (leaky) straight waveguide. In [15] conformal mapping with perfectly matched layer (PML) boundary conditions is used to analyze bent waveguides. In a perturbational approach [16] the curvature is treated as a perturbation of a straight waveguide, and the bent waveguide modes are expressed in terms of straight waveguide fields. Other techniques of a more analytical character (e.g. WKB approximations [17], a transfer matrix approach [18]), or of a numerical nature (e.g. beam propagation [19], the method of lines [20], finite difference [21] or finite element discretizations [22]) are applied as well.

The pure analytic approach for modeling of optical bent slab waveguides is quite well known [23, 24, 25], though apparently hardly ever evaluated rigorously. When trying to do so, a major obstacle is encountered in the

---

<sup>1</sup>Partly these notions originate from the use of a ray picture for the description of bent waveguides, or from approximate models in terms of “equivalent” leaky straight waveguide profiles. We will avoid these viewpoints in the present paper.

form of the necessity to compute Bessel functions of large complex order and large argument; we experienced that efficient facilities for these function evaluations are not provided by the standard numerical libraries. To overcome that hindrance, most authors resorted to approximations of the problem, such that reliable results for bent slab waveguides, e.g. for the purpose of a bend mode solver benchmark, still seem to be rare.

Using the uniform asymptotic expansions of Bessel functions as provided in Ref. [26], we found that with present standard computers it is not a problem to carry out the rigorous analytic evaluation of the problem. Section 2 introduces the bend mode ansatz and outlines the analytic steps towards a solution. Remarks on bend mode normalization and on orthogonality properties of bend modes are added in Sections 2.1 and 2.2. Section 3 summarizes the results of the analytic model for a series of bend configurations, including a comparison with benchmark results where available.

The present discussion is concerned with a frequency domain model where the (real valued) frequency or vacuum wavelength is regarded as a given parameter, and where one is interested in solutions of the Maxwell equations for wave propagation along angular segments of the curved structures, that are characterized by a complex valued propagation constant. Alternatively, one can consider time-domain resonances that are supported by full circular cavities. In that viewpoint the field solutions are parameterized by an integer azimuthal index; the frequency takes the role of a complex valued eigenvalue. Any difficulties with the complex order Bessel functions are avoided in that way, and the values for frequencies and propagation constants can be largely translated between the two viewpoints [27]. However, the field solutions obtained in the latter way are not directly useful for applications where one is interested in pieces of bent waveguides only. Also for a microresonator model that combines modal solutions for bent and straight waveguides by means of coupled mode theory integrals, the fixed-frequency bend mode profiles as discussed in this paper are required.

## 2 Bent waveguide model

Consider a bent slab waveguide with the  $y$ -axis as the axis of symmetry as shown in Fig. 1. We assume that the material properties and the fields do not vary in the  $y$ -direction. Being specified by the radially dependent refractive index  $n(r)$  (here  $n$  is piecewise constant), the waveguide can be seen as a structure that is homogeneous along the angular coordinate  $\theta$ . Hence one chooses an ansatz for the bend modes with pure exponential dependence on the azimuthal angle, where the angular mode number is commonly written as a product  $\gamma R$  with a reasonably defined bend radius  $R$ , such that  $\gamma$  can be interpreted as a propagation constant. In the cylindrical coordinate system  $(r, \theta)$ , the functional form (in the usual complex notation) of the propagating electric field  $\mathbf{E}$  and the magnetic field  $\mathbf{H}$  reads

$$\mathbf{E}(r, \theta, t) = (\tilde{E}_r, \tilde{E}_\theta)(r) e^{i(\omega t - \gamma R \theta)}, \quad \mathbf{H}(r, \theta, t) = (\tilde{H}_r, \tilde{H}_\theta)(r) e^{i(\omega t - \gamma R \theta)}, \quad (1)$$

where the  $\sim$  symbol indicates the mode profile,  $\gamma$  is the propagation constant of the bend mode, and  $\omega$  is the angular frequency corresponding to vacuum wavelength  $\lambda$ . Since an electromagnetic field propagating through a bent waveguide loses energy due to radiation,  $\gamma$  is complex valued, denoted as  $\gamma = \beta - i\alpha$ , where  $\beta$  and  $\alpha$  are the real valued phase propagation and attenuation constants.

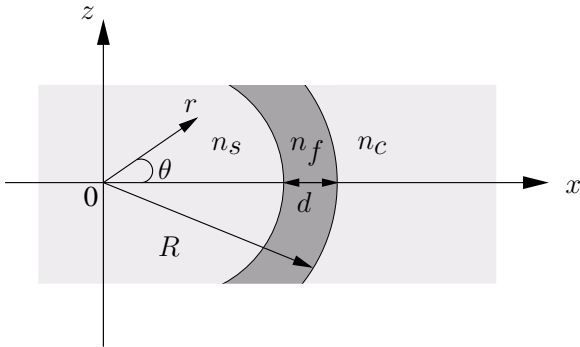


Figure 1: A bent slab waveguide. The core of thickness  $d$  is embedded between an interior medium (“substrate”) with refractive index  $n_s$  and an exterior medium (“cladding”) with refractive index  $n_c$ . The distance between the origin and the outer rim of the bend defines the bend radius  $R$ .

Note that the angular behaviour of the field (1) is determined by the product  $\gamma R$ , where the definition of  $R$  is entirely arbitrary. Given a bend mode, the values assigned to the propagation constant  $\gamma$  change, if the same physical solution is described by using different definitions of the bend radius  $R$ . We will add a few more

comments on this issue in Section 3. The definition of the bend radius  $R$  as the radial position of the outer interface of the core layer is still applicable in case the guiding is effected by a single dielectric interface only, i.e. for the description of whispering gallery modes (see Section 3.5). Hence, for this paper we stick to the definition of  $R$  as introduced in Fig. 1.

If the ansatz (1) is inserted into the Maxwell equations, one obtains the two separate sets of equations

$$\frac{\gamma R}{r} \tilde{E}_y = -\mu_0 \omega \tilde{H}_r, \quad \frac{\partial \tilde{E}_y}{\partial r} = -i\mu_0 \omega \tilde{H}_\theta, \quad \frac{1}{r} \frac{\partial r \tilde{H}_\theta}{\partial r} + \frac{i\gamma R}{r} \tilde{H}_r = -i\epsilon_0 \epsilon \omega \tilde{E}_y \quad (2)$$

and

$$\frac{\gamma R}{r} \tilde{H}_y = \epsilon_0 \epsilon \omega \tilde{E}_r, \quad \frac{\partial \tilde{H}_y}{\partial r} = i\epsilon_0 \epsilon \omega \tilde{E}_\theta, \quad \frac{1}{r} \frac{\partial r \tilde{E}_\theta}{\partial r} + \frac{i\gamma R}{r} \tilde{E}_r = i\mu_0 \omega \tilde{H}_y, \quad (3)$$

with vacuum permittivity  $\epsilon_0$ , vacuum permeability  $\mu_0$ , and the relative permittivity  $\epsilon = n^2$ .

For transverse electric (TE) waves the only nonzero components are  $\tilde{E}_y$ ,  $\tilde{H}_r$  and  $\tilde{H}_\theta$ , which are expressed in terms of  $\tilde{E}_y$ , while for transverse magnetic (TM) waves the only nonzero components are  $\tilde{H}_y$ ,  $\tilde{E}_r$  and  $\tilde{E}_\theta$ , which are given by  $\tilde{H}_y$ . Within radial intervals with constant refractive index  $n$ , the basic electric and magnetic components are governed by a Bessel equation with complex order  $\gamma R$ ,

$$\frac{\partial^2 \phi}{\partial r^2} + \frac{1}{r} \frac{\partial \phi}{\partial r} + (n^2 k^2 - \frac{\gamma^2 R^2}{r^2}) \phi = 0 \quad (4)$$

for  $\phi = \tilde{E}_y$  or  $\phi = \tilde{H}_y$ , where  $k = 2\pi/\lambda$  is the (given, real) vacuum wavenumber. For TE modes, the interface conditions require continuity of  $\tilde{E}_y$  and of  $\partial_r \tilde{E}_y$  across the dielectric interfaces. For TM modes, continuity of  $\tilde{H}_y$  and of  $\epsilon^{-1} \partial_r \tilde{H}_y$  across the interfaces is required.

Eq. (4), together with the interface conditions and suitable boundary conditions for  $r \rightarrow 0$  and  $r \rightarrow \infty$ , represents an eigenvalue problem with the bend mode profiles  $\phi$  as eigenfunctions, and the propagation constants  $\gamma$  or angular mode numbers  $\nu = \gamma R$  as eigenvalues. The equation is solved piecewise in the regions with constant refractive index. While the procedure is in principle applicable for arbitrary multilayer bent waveguides, for the sake of brevity we discuss here the three layer configuration as introduced in Fig. 1.

The general solution of Eq. (4) is a linear combination of the Bessel functions of the first kind  $J$  and of the second kind  $Y$ . This representation is applicable to the core region. Since  $Y$  tends to  $-\infty$  if  $r \rightarrow 0$ , for the boundedness of the electric/magnetic field at the origin one selects only the Bessel function of the first kind  $J$  for the interior region. In the outer region, we are looking for a complex superposition of  $J$  and  $Y$  that represents outgoing waves. Such a solution can be given in terms of the Hankel functions of the first kind  $H^{(1)}$  or of the second kind  $H^{(2)}$ . Using the asymptotic expansions of these functions [26, chap. 9, Eq. (9.2.3), Eq. (9.2.4)]

$$H_\nu^{(1)}(nkr) \sim \sqrt{\frac{2}{\pi nkr}} e^{i(nkr - \nu\pi/2 - \pi/4)}, \quad H_\nu^{(2)}(nkr) \sim \sqrt{\frac{2}{\pi nkr}} e^{-i(nkr - \nu\pi/2 - \pi/4)}, \quad (5)$$

and taking into account the harmonic time dependence  $\exp(i\omega t)$  (with positive frequency), one observes that  $H^{(1)}$  represents incoming waves, while outgoing waves are given by  $H^{(2)}$ . Thus the piecewise ansatz for the basic components of the electric/magnetic bent mode profile is

$$\phi(r) = \begin{cases} A_s J_\nu(n_s k r), & \text{if } 0 \leq r \leq R^-, \\ A_f J_\nu(n_f k r) + B_f Y_\nu(n_f k r), & \text{if } R^- \leq r \leq R^+, \\ A_c H_\nu^{(2)}(n_c k r), & \text{for } r \geq R^+, \end{cases} \quad (6)$$

where  $R^- = R - d$ ,  $R^+ = R$ , and where  $A_s$ ,  $A_f$ ,  $B_f$  and  $A_c$  are so far unknown constants.

The polarization dependent interface conditions lead to a homogeneous system of linear equations for  $A_s$ ,  $A_f$ ,  $B_f$  and  $A_c$ . The condition for a nontrivial solution can be given the form

$$\frac{J_\nu(n_f k R^-)}{J_\nu(n_s k R^-)} - q_s \frac{J'_\nu(n_f k R^-)}{J'_\nu(n_s k R^-)} = \frac{J_\nu(n_f k R^+)}{H_\nu^{(2)}(n_c k R^+)} - q_c \frac{J'_\nu(n_f k R^+)}{H_\nu^{(2)'}(n_c k R^+)} \quad (7)$$

$$\frac{Y_\nu(n_f k R^-)}{J_\nu(n_s k R^-)} - q_s \frac{Y'_\nu(n_f k R^-)}{J'_\nu(n_s k R^-)} = \frac{Y_\nu(n_f k R^+)}{H_\nu^{(2)}(n_c k R^+)} - q_c \frac{Y'_\nu(n_f k R^+)}{H_\nu^{(2)'}(n_c k R^+)}$$

with  $q_j = n_f/n_j$  for TE polarization, and with  $q_j = n_j/n_f$  for TM polarized fields, for  $j = s, c$ . Eq. (7) is the dispersion equation for the three layer bent slab waveguide. For given frequency  $\omega$ , this equation is to be solved<sup>2</sup> for the propagation constants  $\gamma = \nu/R$ .

For the numerical implementation, Eq. (7) is rearranged as

$$T_1 \cdot T_2 = T_3 \cdot T_4, \quad (8)$$

where

$$\begin{aligned} T_1 &= J_\nu(n_f k R^-) J'_\nu(n_s k R^-) - q_s J_\nu(n_s k R^-) J'_\nu(n_f k R^-), \\ T_2 &= Y_\nu(n_f k R^+) H_\nu^{(2)'}(n_c k R^+) - q_c H_\nu^{(2)}(n_c k R^+) Y'_\nu(n_f k R^+), \\ T_3 &= Y_\nu(n_f k R^-) J'_\nu(n_s k R^-) - q_s J_\nu(n_s k R^-) Y'_\nu(n_f k R^-), \\ T_4 &= J_\nu(n_f k R^+) H_\nu^{(2)'}(n_c k R^+) - q_c H_\nu^{(2)}(n_c k R^+) J'_\nu(n_f k R^+). \end{aligned}$$

In contrast to common notions about leaky modes, the fields obtained by the ansatz (6) do not diverge for large radial coordinate  $r$ . The asymptotic expansion (5) predicts a decay  $\sim 1/\sqrt{r}$ . No difficulties related to ‘large’ terms are to be expected for the numerical evaluation of Eq. (8). Moreover, as shown below, with the squared mode profile being accompanied by a factor  $r^{-1}$  in the relevant expression, the bend modes can even be normalized with respect to the azimuthal mode power.

## 2.1 Bend mode normalization

The power flow density associated with a bend mode is given by the time averaged Poynting vector  $\mathbf{S}_{av} = \frac{1}{2} \Re(\mathbf{E} \times \mathbf{H}^*)$ . The axial component  $S_{av,y}$  vanishes in the 2-D setting; for TE waves the radial and azimuthal components evaluate to

$$S_{av,r} = \frac{-1}{2\mu_0\omega} \Re \left[ i \tilde{E}_y \frac{\partial \tilde{E}_y^*}{\partial r} \right] e^{-2\alpha R\theta}, \quad S_{av,\theta} = \frac{\beta}{2\mu_0\omega} \frac{R}{r} |\tilde{E}_y|^2 e^{-2\alpha R\theta}, \quad (9)$$

and for TM polarization one obtains

$$S_{av,r} = \frac{1}{2\epsilon_0\epsilon\omega} \Re \left[ \tilde{H}_y^* \frac{\partial \tilde{H}_y}{\partial r} \right] e^{-2\alpha R\theta}, \quad S_{av,\theta} = \frac{\beta}{2\epsilon_0\epsilon\omega} \frac{R}{r} |\tilde{H}_y|^2 e^{-2\alpha R\theta}. \quad (10)$$

The total optical power transported by the mode in the angular direction is given by  $P_\theta(\theta) = \int_0^\infty S_{av,\theta} dr$ . Somewhat surprisingly, this expression can be considerably simplified by using the following formula [28, Section 11.2, Eq. 5],

$$\int C_\mu(kx) D_\nu(kx) \frac{dx}{x} = \frac{kx}{\mu^2 - \nu^2} \{C_\mu(kx) D_{\nu+1}(kx) - C_{\mu+1}(kx) D_\nu(kx)\} + \frac{C_\mu(kx) D_\nu(kx)}{\mu + \nu} \quad (11)$$

where  $C_\mu, D_\nu$  are any cylindrical functions (i.e. functions which are linear combinations of  $J_\mu$  and  $Y_\mu$ , or of  $J_\nu$  and  $Y_\nu$ , respectively). Observing that for a valid mode profile the pieces of the ansatz (6) satisfy the polarization dependent continuity conditions at the dielectric interfaces, application of Eq. (11) and of several standard identities for Bessel functions leads to exact cancellation of the boundary terms that arise in the piecewise integration, with the exception of the limit term for  $r \rightarrow \infty$ . In that regime the mode profile is represented by the asymptotic form (5) of the relevant Hankel functions, such that one arrives at the two expressions

$$P_\theta(\theta) = \frac{|A_c|^2}{2\mu_0\omega\alpha R\pi} e^{\alpha R(\pi - 2\theta)} \quad (\text{TE}), \quad P_\theta(\theta) = \frac{|A_c|^2}{2\epsilon_0 n_c^2 \omega \alpha R\pi} e^{\alpha R(\pi - 2\theta)} \quad (\text{TM}), \quad (12)$$

<sup>2</sup>In an alternative approach where one looks at time domain resonances of circular cavities, a similar procedure as outlined here [5, 27] leads to precisely the same equation (cf. the remarks in the introduction). In that case Eq. (7) is to be solved for complex valued resonance frequencies  $\omega$ , for given integer azimuthal mode numbers  $\nu$ .

for the modal power of TE and TM polarized modes, respectively. All mode profiles shown in Section 3 are power normalized with respect to these expressions (evaluated at  $\theta = 0$ ).

Alternatively, Eqs. (12) can be derived in a way quite analogous to what follows in Section 2.2: Upon integrating the vanishing divergence of the Poynting vector  $\nabla \cdot (\mathbf{E} \times \mathbf{H}^* + \mathbf{E}^* \times \mathbf{H}) = 0$  for a modal solution  $(\mathbf{E}, \mathbf{H})$  over a differential angular segment in the domain of polar coordinates, by means of Gauss' theorem one relates the angular decay of modal power to the outflow of optical power in the radial direction. The limit of that flow for large radial coordinates exists and can be evaluated by again using the asymptotic form (5) of the mode profile, leading to expressions (12) for the modal power.

By considering the above expressions for large bend radii, one might wonder whether these may lead to a scheme for the normalization of nonguided modal solutions associated with straight waveguides e.g. as given in [29] in terms of plane wave superpositions. Examination of Eq. (12) with the help of Eq. (25), however shows that the expression (12) for the modal power is not applicable in the limit  $R \rightarrow \infty$ . Hence in this respect, there is no direct correspondence between the present bend modes supported by structures with low curvature and radiative modes of similar straight waveguides.

## 2.2 Orthogonality of bend modes

If the bend mode profiles are employed as basis elements for an expansion of a general optical field in the bend structure, the orthogonality properties of these modes become relevant: Projecting on the basis modes allows to relate the modal amplitudes to the given arbitrary field. As a consequence of the leaky nature of the complex bend modes, the orthogonality relations involve nonconjugate versions of the field profiles.<sup>3</sup>

Let  $(\mathbf{E}_p, \mathbf{H}_p)$  and  $(\mathbf{E}_q, \mathbf{H}_q)$  be the electromagnetic fields (1) of bend modes with propagation constants  $\gamma_p$  and  $\gamma_q$ , respectively, that are supported by the same bent waveguide. We start with the identity

$$\nabla \cdot (\mathbf{E}_p \times \mathbf{H}_q - \mathbf{E}_q \times \mathbf{H}_p) = 0, \quad (13)$$

which is a straightforward consequence of the Maxwell equations.

Consider the integral of Eq. (13) over an angular segment  $\Omega = [0, \tilde{r}] \times [\theta, \theta + \Delta\theta]$  in the waveguide plane, specified by intervals of the polar coordinates:

$$\int_{\Omega} \nabla \cdot \mathbf{A} dS = 0, \quad \text{with} \quad \mathbf{A} = (A_r, A_y, A_{\theta}) = \mathbf{E}_p \times \mathbf{H}_q - \mathbf{E}_q \times \mathbf{H}_p. \quad (14)$$

After simplification of Eq. (14) by means of the Gauss theorem and a Taylor series expansion around  $\theta$ , for small, nonzero  $\Delta\theta$  one obtains

$$i(\gamma_p + \gamma_q)R \int_0^{\tilde{r}} A_{\theta}(r, \theta) dr = \tilde{r} A_r(\tilde{r}, \theta). \quad (15)$$

In order to evaluate the limit  $\tilde{r} \rightarrow \infty$  of the right hand side,  $r A_r$  is expressed in terms of the basic mode profile components  $E_y$  and  $H_y$ , with the help of Eqs. (2, 3):

$$r A_r = \frac{i}{\mu_0 \omega} r (E_{p,y} \partial_r E_{q,y} - E_{q,y} \partial_r E_{p,y}) + \frac{i}{\epsilon_0 \epsilon_c \omega} r (H_{p,y} \partial_r H_{q,y} - H_{q,y} \partial_r H_{p,y}). \quad (16)$$

Here  $\epsilon_c = n_c^2$  is the permittivity in the exterior region of the bend (constant for large radii). In this region, the basic components  $\phi_p = \tilde{E}_{p,y}$  or  $\phi_p = \tilde{H}_{p,y}$  of modal solutions (6) are given by Hankel functions of second kind i.e.  $\phi_p(r) = A_{c,p} H_{\gamma_p R}^{(2)}(n_c k r)$ , which, for large radial coordinate, assume the asymptotic forms

$$\phi_p(r) \sim A_{c,p} \sqrt{\frac{2}{\pi n_c k r}} e^{-i(n_c k r - \gamma_p R \pi/2 - \pi/4)}, \quad \partial_r \phi_p(r) \sim \left( -\frac{1}{2r} - i n_c k \right) \phi_p(r). \quad (17)$$

By using these expressions, the limits  $r \rightarrow \infty$  of the individual parts of Eq. (16) can be shown to vanish

$$\lim_{r \rightarrow \infty} [r(\phi_p \partial_r \phi_q - \phi_q \partial_r \phi_p)] = 0. \quad (18)$$

---

<sup>3</sup>An approximate orthogonality relation involving complex conjugates of one of the mode profiles is derived in Ref. [30], valid in the limit of large bend radius (i.e. for almost straight waveguides).

This leads to the identity

$$(\gamma_p + \gamma_q) \int_0^\infty \mathbf{a}_\theta \cdot (\mathbf{E}_p \times \mathbf{H}_q - \mathbf{E}_q \times \mathbf{H}_p) dr = 0, \quad (19)$$

where  $\mathbf{a}_\theta$  is the unit vector in the azimuthal ( $\theta$ -) direction.

After inspecting Eqs. (2, 3), one readily sees that the fields  $(\mathbf{E}_{\tilde{p}}, \mathbf{H}_{\tilde{p}})$  and the propagation constant  $\gamma_{\tilde{p}}$  with

$$\gamma_{\tilde{p}} = -\gamma_p, E_{\tilde{p},r} = E_{p,r}, E_{\tilde{p},y} = E_{p,y}, E_{\tilde{p},\theta} = -E_{p,\theta}, H_{\tilde{p},r} = -H_{p,r}, H_{\tilde{p},y} = -H_{p,y}, H_{\tilde{p},\theta} = H_{p,\theta} \quad (20)$$

describe a valid modal solution of the bend problem. By writing out the expression (19) for the quantities with indices  $\tilde{p}$  and  $q$ , by applying the transformation (20), and by observing that  $\mathbf{a}_\theta \cdot (\mathbf{E}_{\tilde{p}} \times \mathbf{H}_q - \mathbf{E}_q \times \mathbf{H}_{\tilde{p}}) = \mathbf{a}_\theta \cdot (\mathbf{E}_p \times \mathbf{H}_q + \mathbf{E}_q \times \mathbf{H}_p)$ , Eq. (19) can be given the form

$$(\gamma_p - \gamma_q) \int_0^\infty \mathbf{a}_\theta \cdot (\mathbf{E}_p \times \mathbf{H}_q + \mathbf{E}_q \times \mathbf{H}_p) dr = 0. \quad (21)$$

Motivated by the result (21), we define the following symmetric, complex valued product<sup>4</sup> of two (integrable) electromagnetic fields  $(\mathbf{E}_1, \mathbf{H}_1)$  and  $(\mathbf{E}_2, \mathbf{H}_2)$ , given in the polar coordinate system of the bend structure:

$$\begin{aligned} (\mathbf{E}_1, \mathbf{H}_1; \mathbf{E}_2, \mathbf{H}_2) &= \int_0^\infty \mathbf{a}_\theta \cdot (\mathbf{E}_1 \times \mathbf{H}_2 + \mathbf{E}_2 \times \mathbf{H}_1) dr \\ &= \int_0^\infty (E_{1,r}H_{2,y} - E_{1,y}H_{2,r} + E_{2,r}H_{1,y} - E_{2,y}H_{1,r}) dr. \end{aligned} \quad (22)$$

Obviously, the integrand vanishes if fields of different (2-D) polarizations are inserted, i.e. TE and TM bend modes are orthogonal with respect to (22). One easily checks that the product is also zero, if the forward and backward versions (two fields with their components related by the transformation (20)) of a bend mode are inserted. Finally, according to Eq. (21), two nondegenerate bend modes with propagation constants  $\gamma_p \neq \gamma_q$  that are supported by the same bend structure are orthogonal with respect to the product (22). These formal statements hold for pairs of the fields (1) with the full space and time dependence, for the expressions excluding the time dependence, as well as for pairs of pure mode profiles that depend on the radial coordinate only.

Assuming that for a given bend configuration a discrete, indexed set of nondegenerate modal fields  $(\mathbf{E}_p, \mathbf{H}_p)$  with (pairwise different) propagation constants  $\gamma_p$  is considered, the orthogonality properties can be stated in the more compact form

$$(\mathbf{E}_p, \mathbf{H}_p; \mathbf{E}_q, \mathbf{H}_q) = \delta_{p,q} N_p, \text{ with } N_p = 2 \int_0^\infty \mathbf{a}_\theta \cdot (\mathbf{E}_p \times \mathbf{H}_p) dr = 2 \int_0^\infty (E_{p,r}H_{p,y} - E_{p,y}H_{p,r}) dr, \quad (23)$$

and  $\delta_{p,q} = 0$  for  $p \neq q$ ,  $\delta_{p,p} = 1$ . For mode sets of uniform polarization and uniform direction of propagation, it can be convenient to write the orthogonality properties in terms of the basic mode profile components  $\phi = E_y^0$  (TE) or  $\phi = H_y^0$  (TM). This leads to the relations

$$\int_0^\infty \zeta \frac{\phi_p \phi_q}{r} dr = \delta_{p,q} P_p, \text{ with } P_p = \int_0^\infty \zeta \frac{\phi_p^2}{r} dr, \quad (24)$$

$\zeta = 1$  for TE, and  $\zeta = 1/\epsilon(r)$  for TM polarization, which differ from the corresponding familiar expressions for straight dielectric slab waveguides by the appearance of the inverse radial coordinate  $r$  only. According to Eq. (17),  $P_p$  is obviously bounded. Note, however, that here  $N_p$  and  $P_p$  are complex valued quantities.

An alternative derivation of Eq. (24) starts with the eigenvalue equation (4), written out for two different modal solutions. Each equation is multiplied by the other mode profile, one subtracts the results, and integrates over the radial axis. This leads to an equation with the difference of the squared propagation constants times the integral of Eq. (24) on one side, and with a limit as in Eq. (16) on the other. Then the reasoning of Eqs. (17, 18) can be applied to obtain the desired result. All sets of bend mode profiles shown in the following sections satisfy the relations (23) or (24), respectively, up to the accuracy that can be expected from the computational procedures.

<sup>4</sup>Cf. the standard variants of orthogonality relations for straight dielectric waveguides made of attenuating materials, as introduced e.g. in Ref. [25]

### 3 Examples

The solution of Eq. (7) requires the evaluation of Bessel and Hankel functions of complex order, where typically values of  $\nu = \gamma R$  in intervals  $\Re(\nu) \in [10^1, 10^4]$  and  $\Im(\nu) \in [-10^{-1}, -10^{-12}]$  and arguments  $nkr$  up to  $10^5$  are encountered. The relevant Bessel functions are well behaved for the above values of order and argument; in particular, no terms with numerically harmful growth appear. We found that subroutines for complex order Bessel functions are not included in standard numerical libraries, therefore we had to resort to own implementations. The procedures are based on ‘uniform asymptotic expansions’ of Bessel functions and their derivatives in terms of Airy functions [26], [31]. More specifically, Eqs. 9.3.35, 9.3.36, 9.3.43, 9.3.44 from Ref. [26] were encoded, restricted to the first two terms of the summations, which we observed to be sufficient for the present examples. Routines for Airy functions with complex arguments according to Ref. [32] were adopted. Further details can be found in Refs. [33], [34].

The expansions are not applicable in a regime where the order is close to the argument of the cylindrical functions. Fortunately we are interested here in configurations that involve complex orders ( $\gamma R$ ) with negative imaginary parts ( $-\alpha$ ), and real arguments ( $nkr$ ). While cases with approximate equality of order and argument could in principle occur for bend modes with extremely low loss, for the evaluation of propagation constants and the profile plots of the examples below this transition region appeared not to be relevant. Otherwise, supplementary routines (see e.g. [31]) would have to be incorporated that cover that region of parameters.

Two techniques were implemented to find the roots  $\nu$  of Eq. (7) in the complex plane. As a heuristic search procedure, a suitably selected region of the complex plane is divided into a number of rectangles, the lower left and upper right corner points of which are then supplied as initial guesses to a root finding routine based on the secant method. Repeated roots are rejected, the remaining unique roots are sorted in descending order of their imaginary part  $-\alpha$ . By refining the subdivision into rectangles, it can be ascertained with reasonable robustness that all the roots in the given region are captured.

Alternatively, a root tracking procedure is implemented to solve the dispersion equation. Starting with the propagation constants of straight waveguides with a refractive index profile cross section equal to that of the given bent waveguide, a series of bends with decreasing radius are considered, with the roots found for each configuration used as initial guesses for the subsequent one. In this way, the bend propagation constants are followed in the complex plane.

Modes of different orders are indexed by counting the local minima in the absolute value of the principal electric (TE) or magnetic (TM) component of the mode profile.

#### 3.1 Propagation constants

For purposes of validating our implementation we start with a comparison of phase propagation constants and attenuation levels. Tables 1 and 2 list values for angular mode numbers obtained with the present mode solver for two bend configurations adopted from Ref. [25], together with reference data from that source. We found an excellent overall agreement, for both the configurations with higher (Table 1) and lower refractive index contrast (Table 2).

$R$ [ $\mu\text{m}$ ]	$\nu = \gamma' R'$ , Ref. [25]	$\nu = \gamma R$ , present
50.5	$4.0189 \cdot 10^2 - i 7.9990 \cdot 10^{-2}$	$4.0189 \cdot 10^2 - i 7.9973 \cdot 10^{-2}$
100.5	$8.0278 \cdot 10^2 - (i 1.2856 \cdot 10^{-2})$	$8.0278 \cdot 10^2 - i 9.6032 \cdot 10^{-4}$
150.5	$1.2039 \cdot 10^3 - i 7.3948 \cdot 10^{-6}$	$1.2039 \cdot 10^3 - i 7.3914 \cdot 10^{-6}$
200.5	$1.6051 \cdot 10^3 - i 4.9106 \cdot 10^{-8}$	$1.6051 \cdot 10^3 - i 4.8976 \cdot 10^{-8}$

Table 1:  $TE_0$  angular mode numbers  $\nu$  for bent waveguides of different bend radius  $R$  according to Fig. 1, with  $(n_s, n_f, n_c) = (1.6, 1.7, 1.6)$ ,  $d = 1 \mu\text{m}$ , for a vacuum wavelength  $\lambda = 1.3 \mu\text{m}$ . Second column: Results from Ref. [25].

The discussion of bent waveguides in Ref. [25] applies an alternative definition of the bend radius  $R'$  as the distance from the origin to the center of the core layer, which is related to the radius  $R$  as introduced in Fig. 1 by  $R' = R - d/2$  (hence the unusual values of bend radii in Tables 1, 2). Both definitions are meant as descriptions

$R$ [ $\mu\text{m}$ ]	$\nu = \gamma' R'$ , Ref. [25]	$\nu = \gamma R$ , present
200.5	$3.1364 \cdot 10^3 - i 6.2059 \cdot 10^{-1}$	$3.1364 \cdot 10^3 - i 6.2135 \cdot 10^{-1}$
400.5	$6.2700 \cdot 10^3 - i 4.9106 \cdot 10^{-2}$	$6.2700 \cdot 10^3 - i 4.9159 \cdot 10^{-2}$
600.5	$9.4041 \cdot 10^3 - i 2.5635 \cdot 10^{-3}$	$9.4041 \cdot 10^3 - i 2.5636 \cdot 10^{-3}$
800.5	$1.2538 \cdot 10^4 - i 1.1174 \cdot 10^{-4}$	$1.2538 \cdot 10^4 - i 1.1177 \cdot 10^{-4}$
1000.5	$1.5673 \cdot 10^4 - i 4.4804 \cdot 10^{-6}$	$1.5673 \cdot 10^4 - i 7.1806 \cdot 10^{-5}$

Table 2:  $TE_0$  angular mode numbers  $\nu$  for low contrast bends according to Fig. 1, with different bend radius  $R$  and parameters  $(n_s, n_f, n_c) = (3.22, 3.26106, 3.22)$ ,  $d = 1 \mu\text{m}$ , for a vacuum wavelength  $\lambda = 1.3 \mu\text{m}$ . Second column: Results from Ref. [25].

of the same physical configuration, i.e. both lead to the same angular field dependence (1), given in terms of the azimuthal mode numbers  $\nu$  as determined by the dispersion equation (7). Via the relation  $\nu = \gamma R = \gamma' R'$ , the different choices of the bend radius result in different values  $\gamma$  and  $\gamma' = \gamma R / (R - d/2)$  for the propagation constant, and consequently in different values  $\beta$ ,  $\beta'$  and  $\alpha$ ,  $\alpha'$  for the phase and attenuation constants.

Still, for many applications one is interested in the variation of the phase constant and the attenuation with the curvature of the bend, expressed by the bend radius. Fig. 2 shows corresponding plots for the configuration of Table 1, including values for the two different bend radius definitions. While on the scale of the figure the differences are not visible for the attenuation constants, the levels of the phase propagation constants differ indeed substantially for smaller bend radii. As expected, for low curvature the values of both  $\beta/k$  and  $\beta'/k$  tend to the effective indices of straight slab waveguides with equivalent refractive index profile. For the present low contrast configuration, only minor differences between TE and TM polarization occur.

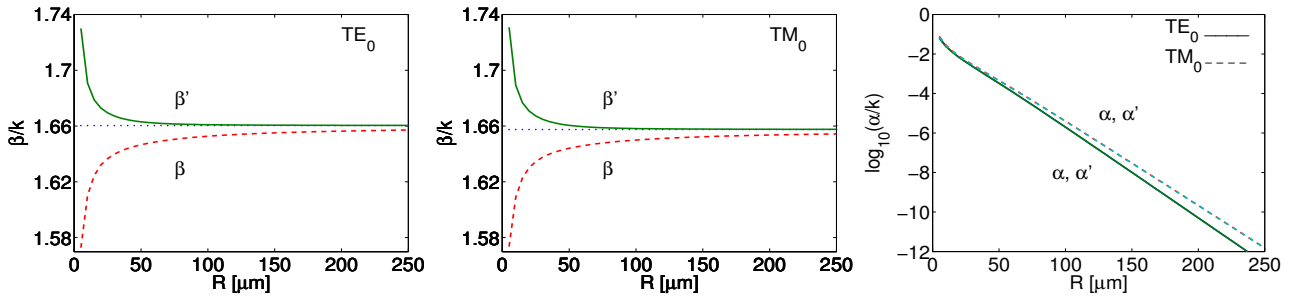


Figure 2: Phase constants  $\beta$ ,  $\beta'$  and attenuation constants  $\alpha$ ,  $\alpha'$  versus the bend radius  $R$ , for bends according to Table 1. The dashed quantities  $\beta' = \beta R / R'$  and  $\alpha' = \alpha R / R'$  correspond to a description of the bend in terms of an alternative bend radius  $R' = R - d/2$ . The dotted lines in the first two plots indicate the levels of the effective indices of a straight waveguide with the cross section and refractive index profile of the bent slabs.

Certainly no physical reasoning should rely on the entirely arbitrary definition of the bend radius. This concerns e.g. statements about the growth or decay of phase propagation constants with  $R$  (according to Fig. 2 the sign of the slope can indeed differ), or discussions about the “phase matching” of bent waveguides and straight channels in coupler or microresonator configurations. Care must be taken that values for  $\beta$  and  $\alpha$  or effective quantities like  $\beta/k$  are used with the proper definition of  $R$  taken into account.

With the present analytic (or semi-analytic) solutions at hand, we have now a possibility to validate “classical” expressions for the variation of the bend attenuation with the bend radius. Beyond the high curvature region, Fig. 2 shows a strict exponential decay of  $\alpha$  with respect to  $R$ , as predicted by an approximate loss formula for symmetric bent slabs given in [35, Eq. 9.6-24]:

$$\alpha = \frac{R - w}{R} \frac{g^2}{2\beta_s(1 + gw)} \frac{h^2}{(n_f^2 - n_s^2)k^2} e^{2gw} e^{-2(\beta_s \tanh^{-1}(g/\beta_s) - g)(R - w)}. \quad (25)$$

Here  $\beta_s$  is the propagation constant corresponding to the straight waveguide with the width  $d = 2w$  and refractive index profile  $(n_s, n_f, n_s)$  of the bent waveguide under investigation. Derived quantities are  $g^2 = \beta_s^2 - n_s^2 k^2$  and  $h^2 = (n_f^2 - n_s^2)k^2 - g^2$ . Fig. 3 reveals a very good agreement with the attenuation constants calculated by our procedures for bends with low curvature.



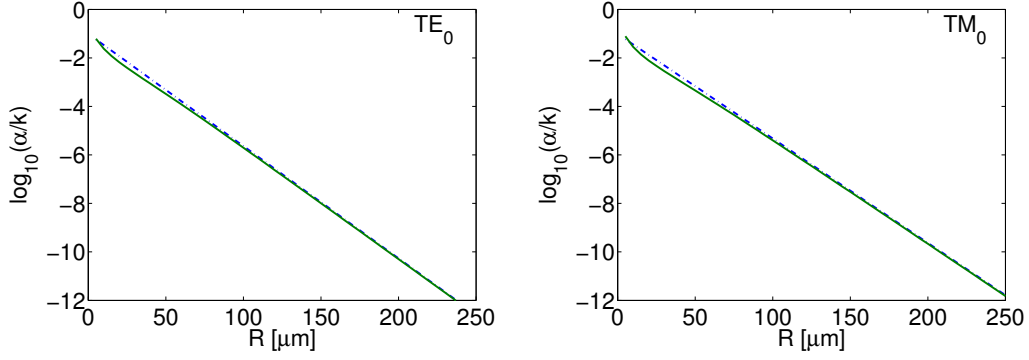


Figure 3: Attenuation constants of the principal TE and TM modes for symmetric bent waveguides with  $n_f = 1.7$ ,  $n_s = n_c = 1.6$ ,  $d = 1 \mu\text{m}$ ,  $\lambda = 1.3 \mu\text{m}$ , for varying bend radius  $R$ . The dashed lines show the exponential decay according to Eq. (25); the solid curves are the present analytic mode solver results.

### 3.2 Mode profiles

Beyond the values of the propagation constants, the present analytical mode solver permits to evaluate modal fields for the full range of radial coordinates. Fig. 4 illustrates normalized profiles for a few fundamental TE bend modes of the configurations considered in Table 1.

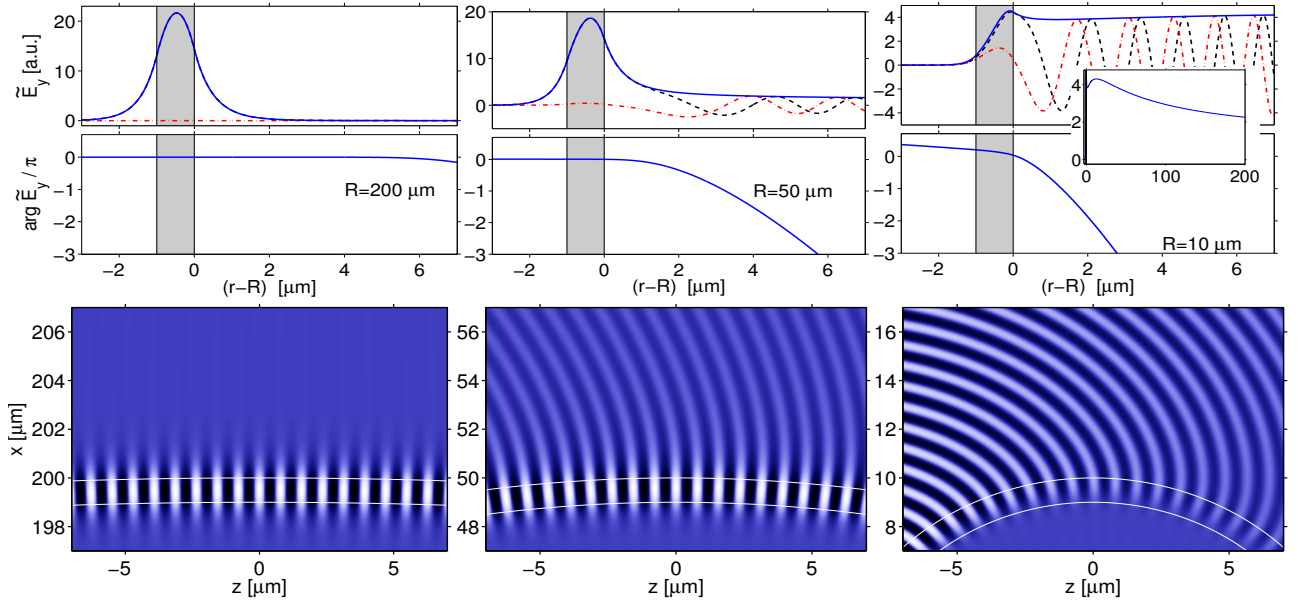


Figure 4:  $TE_0$  mode profiles for bends according to the setting of Table 1, with different bend radii  $R = 200, 50, 10 \mu\text{m}$ . First row: radial dependence of the absolute value (solid line), the real- and imaginary part (dashed and dash-dotted lines), and the phase of the basic electric field component  $\tilde{E}_y$ . The profiles are normalized according to Eq. (12), with the global phase adjusted such that  $\tilde{E}_y(R)$  is real and positive. Second row: snapshots of the propagating bend modes according to Eq. (1). The gray scales correspond to the levels of the real, physical field  $E_y$ .

One observes the expected effects [35, 25]: Bends with large radii  $R$  support modes with almost the familiar symmetric, well confined plane profiles of straight symmetric slab waveguides. With decreasing bend radius, the phase profiles of the bend modes become more and more curved. Along with the increasing attenuation, the maximum in the absolute value of the basic electric field shifts towards the outer rim of the bend, and the relative field levels in the exterior region grow. The mode profiles are essentially complex, with oscillatory behaviour of the real- and imaginary parts of the field profiles in the exterior region. The effects of “bending” and the lossy nature of the bend modes are illustrated best by the snapshots of the physical fields in the second row of Fig. 4.

Just as for straight waveguides, the confinement of the bend modes depends critically upon the refractive index contrast. As exemplified by Fig. 5, one observes quite similar effects when the core refractive index of the

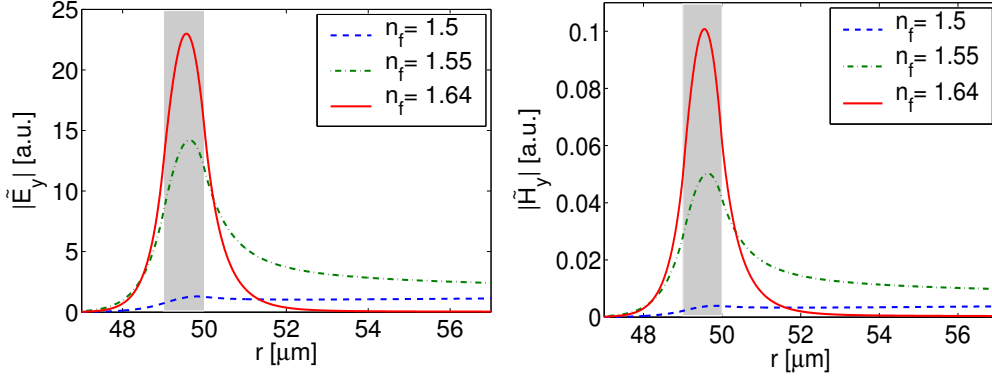


Figure 5: *Fundamental TE (left) and TM mode profiles (right) for symmetric bent slabs with  $R = 50 \mu\text{m}$ ,  $\lambda = 1.55 \mu\text{m}$ ,  $d = 1 \mu\text{m}$ ,  $n_s = n_c = 1.45$ , and different core refractive indices. As  $n_f$  is changed from 1.5 to 1.55 to 1.64, the effective propagation constants  $\gamma/k$  change from  $1.4580 - i 9.2077 \cdot 10^{-3}$  to  $1.4893 - i 1.1624 \cdot 10^{-3}$  to  $1.5598 - i 2.1364 \cdot 10^{-7}$  ( $TE_0$ ), and from  $1.4573 - i 1.0088 \cdot 10^{-2}$  to  $1.4862 - i 1.6013 \cdot 10^{-3}$  to  $1.5504 - i 9.4104 \cdot 10^{-7}$  ( $TM_0$ ), respectively.*

bend is varied, as found for the change in bend radius: With loosened confinement and growing attenuation for decreasing  $n_f$ , the mode profile maximum shifts towards the outer rim, and the relative field levels in the exterior region increase. Note that all (normalizable) mode profiles decay for large radial coordinates according to Eqs. (6) and (17), despite their appearance in Figs. 4 and 5 (See the insets in Figs. 4, 7, 9).

### 3.3 Comparison with FDTD results

As an attempt for a further validation of our results on bend modes we have considered the following numerical experiment. Embedded in a common background, the core of a straight slab waveguide is placed in the vicinity of a ring shaped core of the same width. If a guided wave is launched into the straight channel, by evanescent coupling it excites optical waves that travel around the ring. If, for given polarization, the bent ring waveguide supports only a single low-loss bend mode, one can expect that a field with the corresponding profile establishes itself after a suitable propagation distance. The experiment is carried out in the time domain, with a ramped-up, subsequently time-harmonic excitation, that is advanced over a limited time interval, such that resonance effects can be excluded. Allowing the “wave front” to propagate once around the ring, a radial field cross section e.g. at an angular position of  $90^\circ$  after the in-coupling region can be expected to give an approximation to the bend mode profile. By observing the exponential decay of the “stationary” field for an angular segment after that region, one can estimate the attenuation of the bend mode.

We have applied a standard Finite Difference Time Domain (FDTD) scheme [36], [37], where a computational window of  $80 \times 58 \mu\text{m}^2$  is discretized uniformly by a mesh with step sizes of  $0.05 \mu\text{m}$ . Perfectly matched layer (PML) boundary conditions enclose the computational domain, with a width of 8 points, a quadratic envelope, and a strength such that the theoretical reflectivity of a wave propagating through the background material at normal incidence is  $10^{-6}$ . The interior of the computational window contains the ring with parameters as given for Fig. 6 and the straight waveguide with the same refractive index profile, with a gap of  $0.5 \mu\text{m}$  in between. A modal field is launched into the straight core using the total field /scattered field approach [38]. Its amplitude is raised according to a half-Gaussian curve with a waist of 5 fs, with the maximum being reached at 40 fs. After this time, the incident field amplitude is kept constant. The simulation runs for a time of 1.1 ps with a time step of 0.1 fs, after which the ramp of the wave has gone around the ring approximately once.

Fig. 6 shows an excellent agreement of the approximation for the bend mode profile obtained in this way with the result of the analytical bend mode solver. We also found a very good agreement of the attenuation constant  $\alpha = 0.01949 \mu\text{m}^{-1}$  estimated by the FDTD simulation with the analytic result  $\alpha = 0.01978 \mu\text{m}^{-1}$ . Hence comparisons of this kind can confirm the expectation that the bend modes as introduced in Eq. (1) are indeed suitable basis fields for a (2-D) description of cylindrical microresonator configurations.

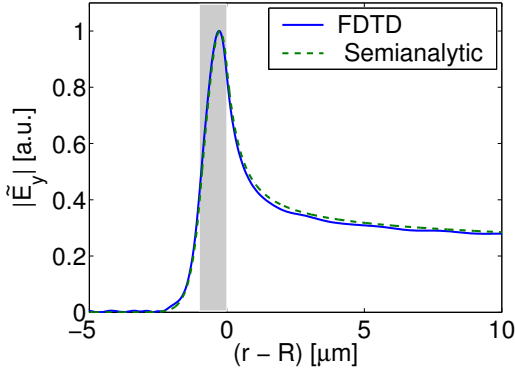


Figure 6: Bend mode profiles as determined by a FDTD simulation (continuous line) and by the analytical model (dashed curve), for a configuration with  $(n_s, n_f, n_c) = (1.6, 1.7, 1.6)$ ,  $d = 1 \mu\text{m}$ ,  $R = 25 \mu\text{m}$ ,  $\lambda = 1.3 \mu\text{m}$ . Here the mode profiles are normalized to a unit maximum.

### 3.4 Higher order bend modes

For cylindrical cavities with relatively high radial refractive index contrast, also higher order bend modes can be relevant for an adequate representation of resonant field patterns [39], [40], [41]. Table 3 summarizes results for propagation constants of fundamental and first order modes of both polarizations for a nonsymmetric slab with decreasing bend radius. In a straight configuration, the refractive index profile supports two guided modes per polarization orientation.

$R [\mu\text{m}]$	$\text{TE}_0$		$\text{TE}_1$		$\text{TM}_0$		$\text{TM}_1$	
	$\beta/k$	$\alpha/k$	$\beta/k$	$\alpha/k$	$\beta/k$	$\alpha/k$	$\beta/k$	$\alpha/k$
$\infty$	1.6775	—	1.6164	—	1.6758	—	1.6134	—
150	1.6663	$\approx 0$	1.6037	$1.2117 \cdot 10^{-7}$	1.6645	$\approx 0$	1.6004	$3.5259 \cdot 10^{-7}$
100	1.6611	$1.0984 \cdot 10^{-12}$	1.5979	$1.7606 \cdot 10^{-5}$	1.6593	$1.8446 \cdot 10^{-12}$	1.5946	$3.4692 \cdot 10^{-5}$
50	1.6473	$9.6704 \cdot 10^{-7}$	1.5818	$1.5113 \cdot 10^{-3}$	1.6451	$1.2668 \cdot 10^{-6}$	1.5791	$2.0368 \cdot 10^{-3}$
20	1.6185	$1.8299 \cdot 10^{-3}$	1.5283	$1.4205 \cdot 10^{-2}$	1.6156	$2.1391 \cdot 10^{-3}$	1.5273	$1.7868 \cdot 10^{-2}$
10	1.5890	$1.6025 \cdot 10^{-2}$	1.4381	$3.4287 \cdot 10^{-2}$	1.5855	$1.8702 \cdot 10^{-2}$	1.4391	$4.6089 \cdot 10^{-2}$

Table 3: Propagation constants  $\gamma = \beta - i\alpha$  of fundamental and first order modes for bends with  $(n_s, n_f, n_c) = (1.6, 1.7, 1.55)$ ,  $d = 2 \mu\text{m}$ ,  $\lambda = 1.55 \mu\text{m}$ , for different bend radii  $R$ . The value  $R = \infty$  indicates the corresponding (bimodal) straight waveguide.

Just as for the fundamental fields, the attenuation of the first order modes grows with decreasing bend radius. Fig. 7 shows that the significantly higher loss levels of the first order modes are accompanied by larger field amplitudes in the exterior region and by a wider radial extent of the mode profiles.

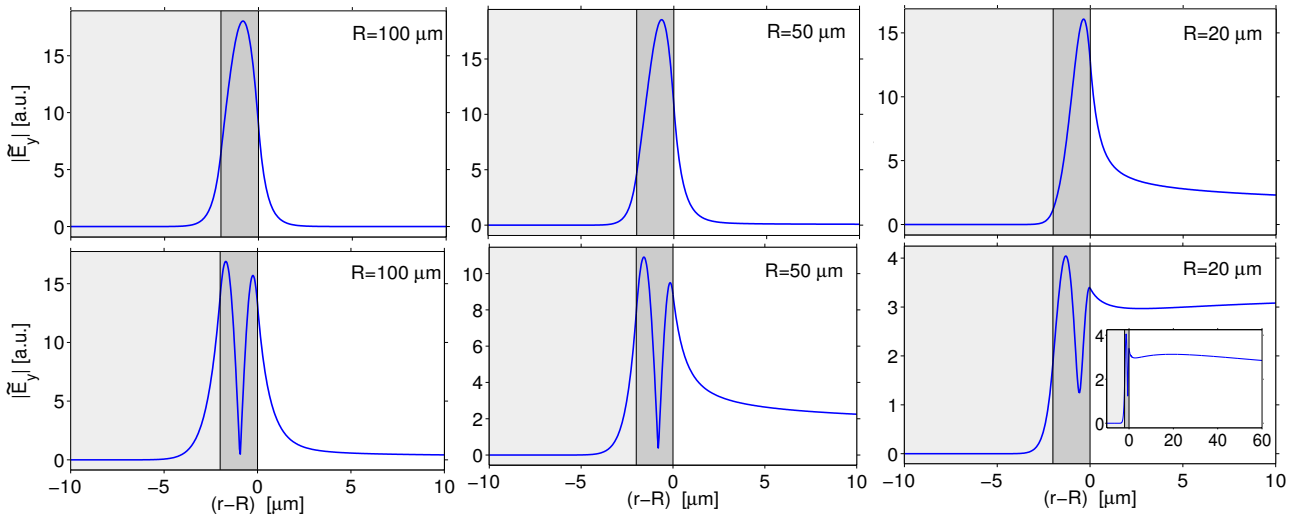


Figure 7: Fundamental and first order TE modes for the bends of Table 3, absolute values of the basic profile component  $\tilde{E}_y$  of structures with radii  $R = 100, 50$ , and  $20 \mu\text{m}$ .

Fig. 8 illustrates the spatial evolution of the  $\text{TE}_0$  and  $\text{TE}_1$  modes for a small configuration with  $R = 20 \mu\text{m}$ . Major differences between the plots for the single fundamental and first order fields are the faster decay of the  $\text{TE}_1$  mode and the minimum in the radial distribution of that field. The last column of Fig. 8 gives an example

for an interference pattern that is generated by a superposition of both modes. Normalized profiles with unit amplitudes and real, positive  $\tilde{E}_y(R)$  are initialized at  $\theta = 0$ , or  $z = 0$ , respectively (cf. Fig. 1). In the core region one observes the familiar beating process, here in the angular direction, with intensity maxima shifting periodically between the center and the outer rim of the ring. In the exterior region, the mode interference results in a ray-like pattern, where rapidly diverging bundles of waves propagate in directions tangential to the ring, originating from regions around the intensity maxima at the outer ring interface. These phenomena are obscured by the fast decay of the first order mode.

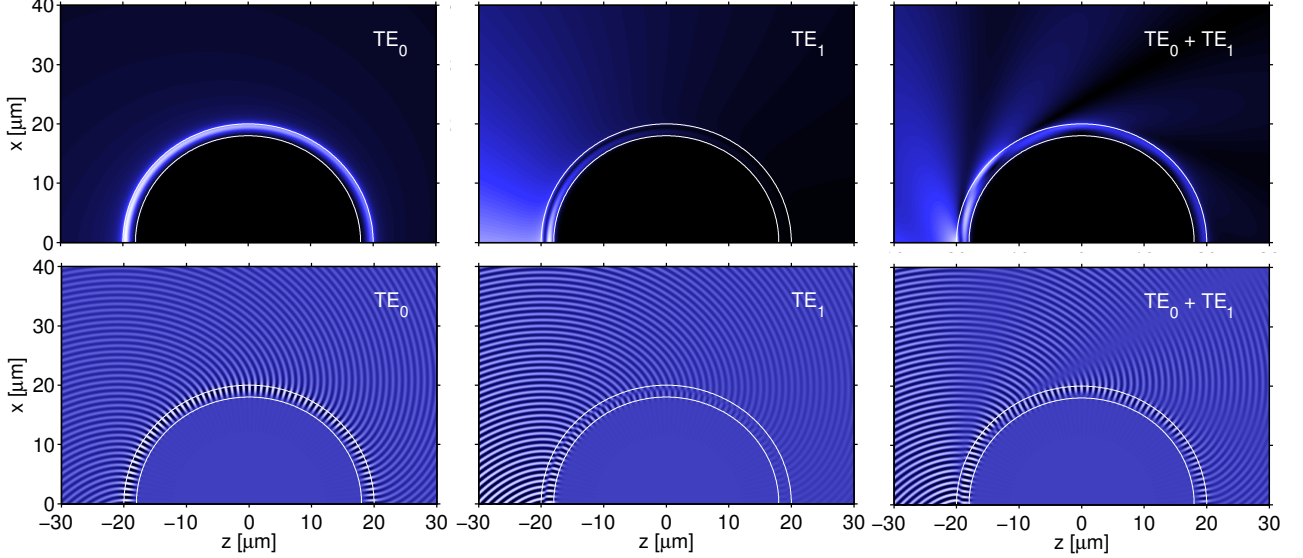


Figure 8: *Spatial evolution and interference of the fundamental and first order TE modes, for a configuration of Table 3 with  $R = 20 \mu\text{m}$ . The propagation of the  $\text{TE}_0$  mode (left), of the  $\text{TE}_1$  mode (center), and of a superposition of these (right) is evaluated. The plots show the absolute value  $|E_y|$  (top) and snapshots of the time harmonic physical field  $E_y$  (bottom).*

Apart from the fundamental and first order fields, further higher order modes can be found for the bent slabs of Table 3. While the  $\text{TE}_0$  and  $\text{TE}_1$  modes considered so far can be viewed as being related to the guided modes supported by a straight slab with the same refractive index profile and thickness, the profiles shown in Fig. 9 are not related to guided modes of that straight waveguide. The classification by the number of minima in the absolute value of the mode profile can still be applied; also the systematics of larger attenuation and higher exterior field levels for growing mode order remains valid.

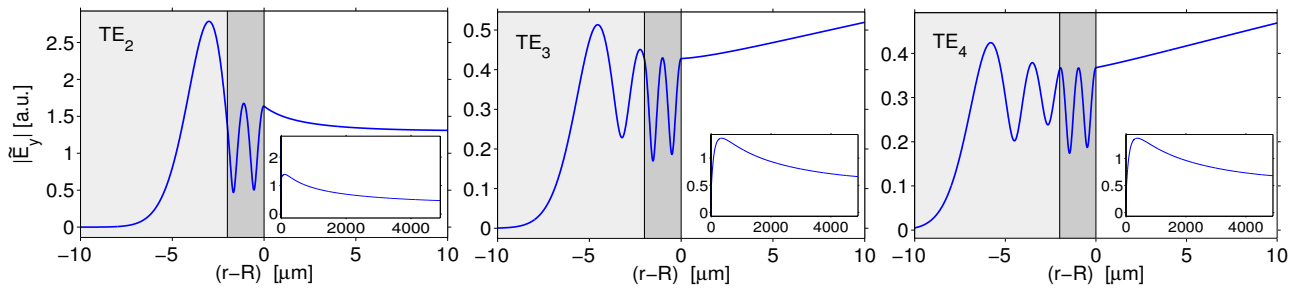


Figure 9: *Higher order TE modes for a bend as considered for Table 3 with  $R = 100 \mu\text{m}$ . The corresponding propagation constants  $\gamma/k$  are  $1.5347 - i 2.8974 \cdot 10^{-3}$  ( $\text{TE}_2$ ),  $1.5094 - i 5.7969 \cdot 10^{-3}$  ( $\text{TE}_3$ ), and  $1.4891 - i 6.1955 \cdot 10^{-3}$  ( $\text{TE}_4$ ), respectively. The insets clearly show the decay of the mode profiles for  $r \rightarrow \infty$  after an initial growth of the field in the cover region.*

In contrast to the two lowest order fields, these higher order modes exhibit pronounced intensity maxima in the interior region. Apparently, for the present nonsymmetric bend, this indicates the transition to the regime of whispering gallery modes, which is discussed below.

### 3.5 Whispering gallery modes

In contrast to the case of straight configurations, localized optical waves can propagate along a single curved dielectric interface. The model of Section 2 covers those configurations with the formal choice  $n_s = n_f$  in Fig. 1, where  $d$  becomes irrelevant. A corresponding ansatz for the mode profile analogous to (6) with merely two pieces leads to a dispersion equation that is considerably simpler than Eq. (7). Table 4 and Fig. 10 summarize results for propagation constants and profiles of these whispering gallery modes.

	$\gamma/k$ , present	$\gamma/k$ , Ref. [42]
TE <sub>0</sub>	$1.3106 - i 1.1294 \cdot 10^{-5}$	$1.310 - i 1.133 \cdot 10^{-5}$
TE <sub>1</sub>	$1.1348 - i 1.8862 \cdot 10^{-3}$	$1.134 - i 1.888 \cdot 10^{-3}$
TE <sub>2</sub>	$0.9902 - i 1.1676 \cdot 10^{-2}$	—
TE <sub>3</sub>	$0.8558 - i 1.8832 \cdot 10^{-2}$	—

Table 4: *Propagation constants  $\gamma$  for the whispering gallery modes of a curved dielectric interface with the parameters  $n_f = 1.5$ ,  $n_c = 1.0$ ,  $R = 4.0 \mu\text{m}$ , and  $\lambda = 1.0 \mu\text{m}$ . Third column: Results from Ref. [42].*

For this example we adopted a set of parameters from Ref. [42], that specifies a high-contrast curved interface with a rather small radius, i.e. a parameter regime that differs considerably from the previous bent slabs. Still, for growing mode order, qualitatively one finds the increase of the attenuation, the outwards shift of the outermost profile intensity maxima, the raise of the exterior field levels, and the wider radial extent of the profiles, just as for the modes of the bent cores in Figs. 7 and 9. In contrast to the impression given e.g. in Refs. [39], [41], the complex mode profiles exhibit minima in the absolute value of the principal field component, not nodal points.

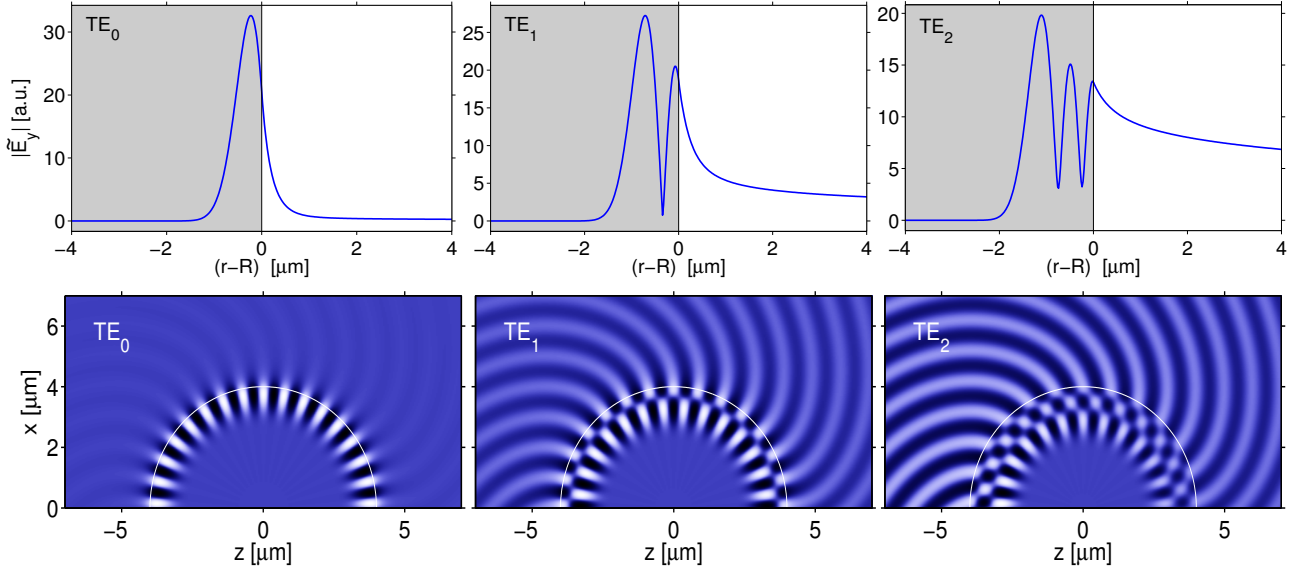


Figure 10: *Profiles (top) and physical field evolution (bottom) of the three lowest order whispering gallery modes according to the specification of Table 4.*

Despite the substantial differences in the attenuation levels of these modes, the higher order fields may well play a role for the representation of resonances of the corresponding disc-shaped microresonator cavity, due to the rather short circumference. Therefore we conclude this paper with two examples of interferences of whispering gallery modes in Fig. 11. As for the bend slabs in Fig. 8 one observes an interior beating pattern and ray-like bundles of waves in the exterior, here on much shorter ranges in terms of the local wavelength.

## 4 Concluding remarks

In this paper we have reconsidered a classical rigorous analytic model for 2-D optical bent slab waveguides and curved dielectric interfaces with piecewise constant refractive index profiles. A frequency domain ansatz in terms of complex order Bessel and Hankel functions leads to an eigenvalue equation (transverse resonance condition) that is to be solved for the complex valued angular mode number.

According to the asymptotic expansions of the relevant Hankel functions, the modal solutions decay according



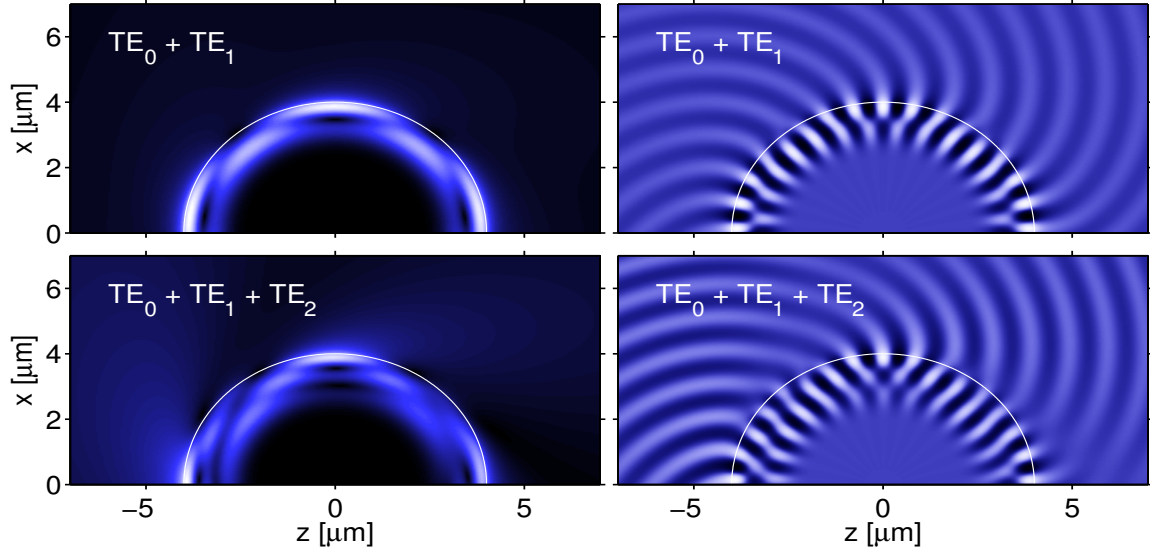


Figure 11: *Interference patterns of the modes of Fig. 10 and Table 4; the plots show the absolute value  $|E_y|$  (left) and snapshots of the time harmonic physical field  $E_y$  (right). Superpositions of the two (top) and three (bottom) lowest order fields are considered, initialized with unit amplitudes of the normalized profiles (with positive  $\tilde{E}_y(R)$ ) at  $z = 0$ .*

to  $1/\sqrt{r}$  for growing radial coordinates  $r$ , i.e. specific products of the profile components are integrable along the radial axis. For purposes of bend mode normalization, we could derive quite compact expressions for the angular modal power. A complex valued product of two general fields in the polar coordinate system has been defined, which is suitable to express orthogonality properties of nondegenerate, directional, and polarized modal solutions of the bent waveguide problem.

A series of detailed (benchmark-) examples complements the former abstract reasoning. Concerning propagation constants, these emphasize the arbitrariness in the definition of the bend radius. Examples for profiles of bend modes and for the spatial evolution of the related physical fields are given, for fundamental and higher order modes of bent slabs with relatively small refractive index contrast, as well as for whispering gallery modes supported by high-contrast curved interfaces. A few illustrative examples for interferences of bend modes have been shown, that exhibit a periodic angular beating pattern (apart from the mode decay) in the guiding regions of the bends, and tangential, ray-like bundles of outgoing waves in the exterior regions.

With the present results, a sound analytical basis for (2-D) coupled-mode-theory modeling of resonator devices involving microrings or microdisks as cavities has been established. We expect that many of the notions of this paper are directly transferable to the case of 3-D configurations involving bent channels with 2-D cross sections.

## 5 Acknowledgements

Financial support by the European Commission (project IST-2000-28018, ‘NAIS’) is gratefully acknowledged. The authors thank E. van Groesen, H. J. W. M. Hoekstra, and the colleagues in the NAIS project for many fruitful discussions on the subject.

## References

- [1] B. E. Little, S. T. Chu, H. A. Haus, J. Foresi, and J.-P. Laine. Microring resonator channel dropping filters. *Journal of Lightwave Technology*, 15(6):998–1005, 1997.
- [2] M. Bertolotti, A. Driessen, and F. Michelotti, editors. *Microresonators as building blocks for VLSI photonics*, volume 709 of AIP conference proceedings. American Institute of Physics, Melville, New York, 2004.

- [3] Next-generation active integrated optic subsystems, project start: 2001. Information society technologies programme of the European Commission, project IST-2000-28018, <http://www.mesaplustwente.nl/nais/>.
- [4] D. G. Hall and B. J. Thompson, editors. *Selected Papers on Coupled-Mode Theory in Guided-Wave Optics*, volume MS 84 of *SPIE Milestone Series*. SPIE Optical Engineering Press, Bellingham, Washington USA, 1993.
- [5] D. R. Rowland and J. D. Love. Evanescent wave coupling of whispering gallery modes of a dielectric cylinder. *IEE Proceedings, Pt. J*, 140(3):177–188, 1993.
- [6] D. J. W. Klunder, E. Krioukov, F. S. Tan, T van der Veen, H. F. Bulthuis, G. Sengo, C. Otto, H. W. J. M. Hoekstra, and A. Driessen. Vertically and laterally waveguide-coupled cylindrical microresonators in  $Si_3N_4$  on  $SiO_2$  technology. *Applied Physics B*, 73:603–608, 2001.
- [7] M. Hammer, K. R. Hiremath, and R. Stoffer. Analytical approaches to the description of optical microresonator devices. In M. Bertolotti, A. Driessen, and F. Michelotti, editors, *Microresonators as building blocks for VLSI photonics*, volume 709 of AIP conference proceedings, pages 48–71. American Institute of Physics, Melville, New York, 2004. Proceedings of the International School of Quantum Electronics, 39th course, Erice, Sicily (October 2003).
- [8] R. Stoffer, K. R. Hiremath, and M. Hammer. Comparison of coupled mode theory and FDTD simulations of coupling between bent and straight optical waveguides. In M. Bertolotti, A. Driessen, and F. Michelotti, editors, *Microresonators as building blocks for VLSI photonics*, volume 709 of AIP conference proceedings, pages 366–377. American Institute of Physics, Melville, New York, 2004. Proceedings of the International School of Quantum Electronics, 39th course, Erice, Sicily (October 2003).
- [9] J. Čtyroký, L. Prkna, and M. Hubálek. Guided-wave optical microresonators: Calculation of eigenmodes. In M. Bertolotti, A. Driessen, and F. Michelotti, editors, *Microresonators as building blocks for VLSI photonics*, volume 709 of AIP conference proceedings, pages 72–90. American Institute of Physics, Melville, New York, 2004. Proceedings of the International School of Quantum Electronics, 39th course, Erice, Sicily (October 2003).
- [10] L. Prkna, M. Hubálek, and J. Čtyroký. Vectorial eigenmode solver for bent waveguides based on mode matching. *IEEE Photonics Technology Letters*, 16(9):2057–2059, September 2004.
- [11] E. A. J. Marcatili. Bends in optical dielectric guides. *The Bell System Technical Journal*, September:2103–2132, 1969.
- [12] D. Marcuse. Bending losses of the asymmetric slab waveguide. *The Bell System Technical Journal*, October:2551–2563, 1971.
- [13] M. Heiblum and J. H. Harris. Analysis of curved optical waveguide by conformal transformation. *IEEE Journal of Quantum Electronics*, 11(2):75–83, 1975.
- [14] F. Wassmann. Modal field analysis of circularly bent single-mode fibers. *IEEE Journal of Lightwave Technology*, 17(5):957–968, 1999.
- [15] P. Bienstman, E. Six, A. Roelens, M. Vanwolleghem, and R. Baets. Calculation of bending losses in dielectric waveguides using eigenmode expansion and perfectly matched layers. *IEEE Photonics Technology Letters*, 14(2):164–166, 2002.
- [16] A. Melloni, F. Carniel, R. Costa, and M. Martinelli. Determination of bend mode characteristics in dielectric waveguides. *IEEE Journal of Lightwave Technology*, 19(4):571–577, 2001.
- [17] W. Berglund and A. Gopinath. WKB analysis of bend losses in optical waveguides. *IEEE Journal of Lightwave Technology*, 18(8):1161–1166, 2000.
- [18] J. M. van der Keur. Propagation properties of a circularly curved, transversely inhomogeneous, dielectric slab waveguide. Technical Report Et/EM 1992-02, Electromagnetic Research Laboratory, Faculty of Electrical Engineering, University of Delft, The Netherlands, 1992.

- [19] M. Rivera. A Finite Difference BPM analysis of bent dielectric waveguides. *IEEE Journal of Lightwave Technology*, 13(2):233–238, 1995.
- [20] R. Pregla. The Method of Lines for the analysis of dielectric waveguide bends. *IEEE Journal of Lightwave Technology*, 14(4):634–639, 1996.
- [21] S. Kim and A. Gopinath. Vector analysis of optical dielectric waveguide bends using finite-difference method. *IEEE Journal of Lightwave Technology*, 14(9):2085–2092, 1996.
- [22] T. Yamamoto and M. Koshiba. Analysis of curvature losses of whispering gallery modes in an optical dielectric disk by the finite-element method. *IEEE Journal of Lightwave Technology*, 12(1):59–63, 1994.
- [23] L. Lewin, D. C. Chang, and E. F. Kuester. *Electromagnetic Waves and Curved Structures*. Peter Peregrinus Ltd. (On behalf of IEE), Stevenage, England, 1977.
- [24] E. C. M. Pennings. *Bends in Optical Ridge Waveguides, Modelling and Experiment*. PhD thesis, Delft University, The Netherlands, 1990.
- [25] C. Vassallo. *Optical Waveguide Concepts*. Elsevier, Amsterdam, 1991.
- [26] M. Abramowitz and I. A. Stegun. *Handbook of Mathematical Functions (Applied Mathematics Series 55)*. National Bureau of Standards, Washington, D.C., 1964.
- [27] L. Prkna, J. Čtyroký, and M. Hubálek. Ring microresonator as a photonic structure with complex eigenfrequency. *Optical and Quantum Electronics*, 36(1-3):259–269, 2004.
- [28] Y. L. Luke. *Integrals of Bessel functions*. McGraw-Hill, New York, 1962.
- [29] P. Benech, D. A. M. Khalil, and F. S. Andr . An exact simplified method for the normalization of radiation modes in planar multilayer structures. *Optics Communications*, 88:96–100, 1992.
- [30] N. Morita and R. Yamada. Electromagnetic fields in circular bends of slab waveguides. *IEEE Journal of Lightwave Technology*, 8(1):16–22, 1990.
- [31] N. M. Temme. Numerical algorithms for uniform Airy-type asymptotic expansions. Technical Report MAS-R9706, Centrum voor Wiskunde en Informatica, Amsterdam, The Netherlands, 1997.
- [32] D. E. Amos. A portable package for Bessel functions of a complex argument and nonnegative order, 1983. <http://www.netlib.org/amos/> .
- [33] K. R. Hiremath. Modeling of 2D cylindrical integrated optical microresonators. Master’s thesis, University of Twente, Enschede, The Netherlands, June 2003.
- [34] L. Prkna. *Rotationally symmetric resonant devices in integrated optics*. PhD thesis, Faculty of Mathematics and Physics, Charles University, Prague, Czech Republic, July 2004.
- [35] D. Marcuse. *Light Transmission Optics*. Van Nostrand Reinhold Company, New York, USA, 1972.
- [36] K. S. Yee. Numerical solution of boundary value problems involving Maxwell’s equations in isotropic media. *IEEE Transactions on Antennas and Propagation*, 14(3):302–307, 1966.
- [37] R. Stoffer, H. J. W. M. Hoekstra, R. M. de Ridder, E. van Groesen, and F. P. H. van Beckum. Numerical studies of 2D photonic crystals: Waveguides, coupling between waveguides and filters. *Optical and Quantum Electronics*, 32:947–961, 2000.
- [38] A. Taflov. *Computational Electrodynamics: The Finite Difference Time Domain Method*. Artech House Inc., Norwood, MA, USA, 1995.
- [39] D.J.W. Klunder, M.L.M. Balisteri, F.C. Blom, J.W.M. Hoekstra, A. Driessen, L. Kuipers, and N.F. Van Hulst. High-resolution photon-scanning tunneling microscope measurements of the whispering gallery modes in a cylindrical microresonator. *IEEE Photonics Technology Letters*, 12(11):1531–1533, 2000.



- [40] M. L. M. Balistreri, D. J. W. Klunder, F. C. Blom, A. Driessen, J. P. Korterik, L. Kuipers, and N. F. van Hulst. Experimental analysis of the whispering gallery modes in a cylindrical optical microcavity. *Journal of the Optical Society of America B*, 18(4):465–471, 2001.
- [41] D. J. W. Klunder, M. L. M. Balistreri, F. C. Blom, H. W. J. M. Hoekstra, A. Driessen, L. Kuipers, and N. F. van Hulst. Detailed analysis of the intracavity phenomena inside a cylindrical microresonator. *IEEE Journal of Lightwave Technology*, 20(3):519–529, 2002.
- [42] R. Stoffer. *Uni- and Omnidirectional Simulation Tools for Integrated Optics*. PhD thesis, University of Twente, Enschede, The Netherlands, May 2001.